Accelerated α Relaxation Dynamics in the Exfoliated Nylon-11/Clay Nanocomposite Observed in the Melt and Semicrystalline State by Dielectric Spectroscopy

Yu-Hsin Lee, Anthony J. Bur,* Steven C. Roth, and Paul R. Start

Polymers Division, National Institute of Standards and Technology, Gaithersburg, Maryland 20899

Received September 21, 2004; Revised Manuscript Received February 11, 2005

ABSTRACT: Melt state properties of nylon-11 and its exfoliated silicate nanocomposite were monitored during extrusion compounding using an on-line dielectric slit die sensor, and solid-state properties were probed off-line below the melting temperature by a dielectric spectrometer. A comprehensive relaxation master map for nylon-11 and its exfoliated clay nanocomposite featuring six relaxation modes in both melt and semicrystalline states revealed changes in molecular dynamics upon the addition of nanofillers. α relaxation was observed in the neat resin as well as the composite, and a Maxwell−Wagner−Sillars (MWS) relaxation was detected in the composite melt yet absent from the neat molten nylon. The MWS relaxation mode, which exhibited a broader relaxation time distribution and a much greater dielectric intensity compared to the α relaxation, resulted from polarization at the filler/polymer interfaces. MWS can be used to distinguish the neat polymer from the composite during real-time processing. The presence of exfoliated clay particles accelerated the α relaxation dynamics in the semicrystalline state as delaminated silicate platelets diminished the intermolecular cooperativity of the amorphous chains. Randomization of molecular dipoles upon increasing temperature was only observed in the neat nylon. Hindered molecular dipole orientation due to the rigid silicate fillers in the nanocomposite was observed.

Introduction

As properties of polymer/clay nanocomposite materials have been extensively explored during the past decade, the dynamics and the segmental motion of polymer chains in the confined clay galleries have gained a growing interest.[1−4] In this article, we report on the application of a new dielectric slit die sensor used to monitor dielectric properties of nylon-11/clay nanocomposite during extrusion from a twin-screw extruder. Data obtained from the amorphous polymer melt using the on-line dielectric sensor are compared with the data acquired from the off-line dielectric measurements in the solid semicrystalline state. How the incorporated nanofillers impact the dielectric relaxation behavior and how the intermolecular cooperativity and dipole orientation of the polymer matrix change due to the presence of delaminated silicate plates are explicitly discussed in this work.

Dielectric relaxation spectroscopy (DRS) is a powerful technique for obtaining molecular dipolar relaxation as a function of temperature and frequency, from which effects due to intermolecular cooperative motion and hindered dipolar rotation can be elucidated. Dielectric relaxations arise when polar segments of the polymer chains are rotated by the application of an alternating electric field. Published experimental studies of dielectric relaxations in semicrystalline polymers disclosed hindered motion in the presence of densely packed crystalline domain.[5−9] The exfoliated or intercalated silicate plates present in the polymer nanocomposites, which serve to segregate the amorphous chains, are analogous to crystallites in the semicrystalline polymers. Thus, hindered dipole rotation is expected to occur in nanocomposite sample, a phenomenon that we study using DRS.

* Corresponding author. E-mail: Anthony.Bur@nist.gov.

For α relaxation, which is associated with the glass transition, it is a process in which a number of amorphous chains relax simultaneously in a cooperative motion. Ideally, the free volume of the polymeric material can expand at high enough temperature to allow most macromolecules to relax individually.[10] On the basis of this argument, much faster chain dynamics should be observed in the melt state compared to the solid semicrystalline state. Nonetheless, polymer molecules relax in a cooperative manner at the temperatures above the glass transition according to the concept proposed by Ngai[11−18] and others.[19−24] Such cooperative chain motion is manifested in the melt where complications due to the crystalline state do not obscure the nature of the dynamics. The concept of intermolecular cooperativity, which is expected to change upon the incorporation of rigid silicate particles, is used in this article to interpret our observations of polymer segmental dynamics.

Previously published studies of nylon-11 and its composites[25−32] serve as a guide for the interpretation of our dielectric observations. On the basis of the cited literature, the following terminologies are adopted: α, amorphous phase relaxation is a macromolecular segmental motion and is associated with the onset of the glass transition;[33−38] α_w, relaxation associated with the movement of extended CH_2 sequences on the backbone with involvement of an amide group which can be facilitated by the presence of water and small plasticizing molecules;[35,38,39] β, relaxation associated with localized motion involving several monomer units, but influenced by hydrogen-bonded amide groups in the presence of water;[35,37−42] γ, relaxation associated with the dynamics of single monomer units;[35,37,39,40] δ, relaxation associated with the dynamics of single monomer units;[35,37,39,40] MWS, Maxwell−Wagner−Sillars relaxation associated with ionic conduction and interfacial polarization occurring between components in the resin

10.1021/ma048052m
Published on Web 03/24/2005

composite having different permittivities;[39,43−45] T_g, glass transition temperature of the amorphous phase, $T_g = 63$ °C (at 3 °C/min by DMA)[31] or $T_g = 40$ °C (at 5 °C/min by DSC)[46] for neat nylon-11.

Experimental Section

1. Sample Preparation. Nylon-11 (Rilsan BESNO) was obtained from Atofina and has a melting temperature of $T_m = 185$ °C. Organically modified clay, Cloisite 30B, was obtained from Southern Clay products and was used as received. Cloisite 30B is produced by ion exchange of natural clay with a methyl, tallow (65% of C18, 30% of C16, and 5% of C14), bis(2-hydroxyethyl), quaternary ammonium ion. Prior to extrusion compounding, the resin and clay powders were dried for 12 h at 80 °C. To prepare 4% mass fraction of clay in the resin, 200 g batches of dry nylon pellets and silicate powders were hand-mixed in a beaker and transferred to a twin-screw extruder feeder. An 18 mm Haake Rheocord model 9000 twin-screw extruder operating at 30 rpm was used. The processing temperature for nylon-11 and its composite was 195 °C. The 30B clay formed a partially exfoliated microstructure with nylon-11 according to the transmission electronic microscopy (TEM) pictures displayed in Figure 1A,B.

2. Instrumentation. The on-line dielectric measurement sensor was recently developed to study dielectric properties of polymer composites in the melt phase.[47] The dielectric cell consists of a flow-through slit, interdigitating electrodes, and standard 12.7 mm (0.5 in.) instrument ports. The cell has a stainless steel housing consisting of top and bottom halves. An alumina ceramic block with interdigitating platinum electrodes that have been fired into the ceramic is placed into the bottom half of the stainless steel housing. A temperature-controlled heating jacket is clamped around the unit. In operation, the dielectric cell is fastened onto the end of the extruder monitoring the resin during flow through the slit. When a voltage (1 V_{rms}) is applied to the interdigitating electrodes, an electric field extends into the molten resin flowing through the slit channel. By measuring the in-phase and out-of-phase components of the current flowing through the resin, the complex relative permittivity, $\epsilon^* = \epsilon' - i\epsilon''$, is measured. The relative standard uncertainty for on-line ϵ' and ϵ'' measurements is 1%. The standard uncertainty of the temperature, which is regulated by the wrap around heating jacket, is 1 °C.

The dielectric cell is connected to a computer-controlled lock-in amplifier (Stanford Research model SR810), which, in conjunction with instrument software, operates as a dielectric spectrometer ("Chemical ElectroPhysics Proceptor") and yields relative permittivity at 14 discrete frequencies from 50 to 10^5 Hz. More details regarding the interdigitating electrode measuring technique and the dielectric slit die design can be found elsewhere.[47−50]

For off-line dielectric measurements of the solid material, the compounded resin extrudate was melt pressed into thin sheets with 0.3−0.8 mm thickness. Aluminum electrodes, 2.54 cm in diameter, were evaporated under vacuum on both sides, followed by storage in an evacuated desiccator. Sample thickness and electrode area were used to calculate the sample vacuum capacitance, C_0. The off-line measurements in the solid state were carried out over a temperature range of −150 to 160 °C. The dielectric sample chamber is a cryostat whose temperature is controlled by the Quatro Cryosystem (Novocontrol) with a resolution of 0.01 °C and stabilization within ±0.05 °C. The sample is fastened between electrical contacts and kept under dry nitrogen gas atmosphere during the measurement. Measurements were performed isothermally in 5 °C increments and 0.2 logarithmic steps in frequency. Dielectric measurements were obtained from 20 Hz to 1 MHz using a precision LCR meter (HP 4284A) at a 1 V_{rms} potential. Data collection was performed in the frequency domain with Novocontrol's WINDETA software after calibrating for open and short connections and correcting for cable impedance. The relative standard uncertainty of ϵ' and ϵ'' from off-line measurements is 0.5%.

Morphological characterization of the composites was carried out by transmission electronic microscopy (TEM). TEM specimens were cut from extruded samples using a Leica cryo-ultramicrotome, equipped with a diamond knife. Sectioning was performed at −80 °C. Sections were collected from the knife edge and placed onto 400 mesh copper−rhodium grids. TEM micrographs were taken with a Philips EM400C at an accelerating voltage of 120 kV.

3. Data Analysis. Polymers contain conducting ions that contribute to both dc conductivity and electrode polarization effects.[47,51] The large increases at low frequencies in both the ϵ' and ϵ'', observed in most polymers at high temperature, are evidences of these two effects and must be corrected for in order to quantify the material dielectric properties. This is accomplished by modeling the electrode as a capacitance/resistance admittance that is in series with the sample and dc conductivity as a resistance in parallel with the sample.[47] The situation can be described as an electrode admittance Y_{el} in series with the sample admittance Y_s.[51] These admittances add to yield the apparent admittance Y_{app}

$$Y_{app} = G_{app} + i\omega C_{app} = \frac{Y_{el}Y_S}{Y_e + Y_S} \tag{1}$$

where G_{app} and C_{app} are the apparent conductance and capacitance and

$$Y_S = G_S + i\omega C_S \tag{2}$$

$$Y_{el} = G_{el} + i\omega C_{el} \tag{3}$$

where the subscripts s and el refer to the sample and electrode, respectively. The dielectric properties of the sample are obtained from eq 2 as

$$\epsilon'_s = \frac{C_s}{C_0} \tag{4}$$

$$\epsilon''_s = \frac{G_s}{\omega C_0} \tag{5}$$

where C_0 is the vacuum capacitance of the sample. In practice, values of the ϵ'_s and ϵ''_s are extracted from Y_{app} by a fitting procedure described as follows.

It is known that the frequency dependence of dielectric relaxations can be described by the Havriliak−Negami (HN) function, which reduces to the Cole−Cole equation for symmetric distributions of relaxation times.[52,53] To analyze the data, a dc conductivity term, proportional to the reciprocal of frequency, was added to a sum of Havriliak−Negami relaxations given as

$$\epsilon^* = \epsilon' - i\epsilon'' = -\frac{i\sigma_{dc}}{\omega\epsilon_0} + \epsilon_\infty + \frac{(\Delta\epsilon)_j}{[1 + (i\omega\tau_j)^{1-\delta_j}]^{\beta_j}} \tag{6}$$

where σ_{dc} is the dc conductivity, $(\Delta\epsilon)_j$ is the strength of the jth dielectric relaxation, δ_j and β_j are the jth relaxation time distribution parameters, ϵ_0 is the permittivity of free space (8.854 pF/m), τ_j is the characteristic relaxation time of the jth relaxation, and ϵ_∞ is the high-frequency relative permittivity. When $\beta = 1$, eq 6 becomes the Cole−Cole equation that describes relaxation with a symmetric distribution of relaxation times. For amorphous polymers, a nonsymmetric distribution of relaxation times is expected for the α relaxation associated with macromolecular segmental motion at temperatures immediately above the glass transition, but for semicrystalline polymers, published data by Boyd,[54−56] Laredo,[35] and others[57−59] show that symmetrical distributions are observed for the relaxation processes. Our initial approach to the analysis was to test for nonsymmetry using the HN equation. We found universally that, in agreement with Boyd and Laredo, the HN parameter $\beta = 1$; i.e., the Cole−Cole

equation is a suitable descriptor of relaxations in nylon-11 and its clay composites.

To analyze the data, the real and imaginary parts of eq 6 are substituted into eq 1 using the definition in eqs 4 and 5. A global fitting procedure consisting of a least-squares nonlinear fit to the frequency-dependent data was carried out using σ_{dc}, $(\Delta\epsilon)_j$, τ_j, δ_j, ϵ_∞, and Y_{el} as fitting parameters. Because the curve-fitting protocol involved the simultaneous fitting to both the real and imaginary parts of the measured dielectric properties and because the initial fitting parameters were determine by isochronal plots such as Figure 4 (presented below) and by published data of others, we were able to minimize fitting errors and avoid fitting artifacts. For on-line measurements, a fit to the data was considered successful if each calculated value was within 1% of the measurement, i.e., within the nominal experimental uncertainty of the observations, and for off-line measurements the fit criterion was 0.5%. For off-line measurements, we found that average curve-fitting errors calculated for each frequency scan were between 0.1% and 0.4%, and for on-line measurements they were between 0.3% and 0.8%. Relaxations with characteristic frequencies that were outside the experimental range were included in the curve-fitting process if their characteristic frequency was within 2 decades of the experimental frequency limit. For the off-line measurements, outlying relaxations were easily identified by extrapolation of the log frequency vs reciprocal temperature plot.

Results and Discussion

1. Measured Dielectric Data. Off-line dielectric measurements on the semicrystalline nylon-11 and nylon-11/30B composite extending over a temperature range from −150 to 120 °C and over frequency from 20 to 10^6 Hz are shown in Figures 2 and 3. The data are divided into low- and high-temperature plots for which several relaxation processes are visible. For temperatures above 90 °C, dc conductivity dominates the dielectric loss ϵ'', and at temperature above 140 °C, electrode polarization effects are seen in ϵ'. Low-frequency dispersions are not visible in the raw data at high temperatures, but by subtracting out dc conductivity and by carrying out curve-fitting analysis, we are able to extract the α relaxation associated with segmental motion of the polymer and a Maxwell−Wagner dispersion associated with polarization of contrasting dielectric interfaces such as resin and clay or crystal and amorphous regions. Dielectric data for the nylon-11/30B composite were obtained over the same temperature and frequency range but are not shown because they are similar to that of the neat polymer, except that the relaxations are shifted on the temperature and frequency scale as is described below.

Before we carried out extensive data analysis and nonlinear curve fitting, we used the measured dielectric loss (ϵ''_{meas}) to establish the number of relaxation maxima and their approximate characteristic frequency. ϵ''_{meas} vs temperature curves at 300 Hz for the neat nylon-11 and its clay composite are plotted in Figure 4. The measured data clearly show the existence of five relaxations that we designate as α, α_w, β, γ, and δ relaxations. The dc conductivity, retrieved from the fitting procedure described above, is subtracted from the raw data, resulting in the two curves that have a maximum labeled α. The estimated peak temperatures for each relaxation process acquired from these dielectric off-line measurements in conjunction with published data for nylon-11 are used as initial values for the nonlinear curve fitting. With the aid of Cole−Cole equation, the overlapping relaxations such as α_w, β, and γ modes illustrated in Figure 4 can be characterized in terms of their relaxation parameters. A Maxwell−Wagner−Sillars (MWS) relaxation, which is known to be present in semicrystalline nylons,[35,36] has its maximum slightly below the lowest frequency of our measurements (20 Hz), but it is a large dispersion and its high-frequency tail extends well into the measurement region, so that the curve-fitting routine (described below) must take it into account.

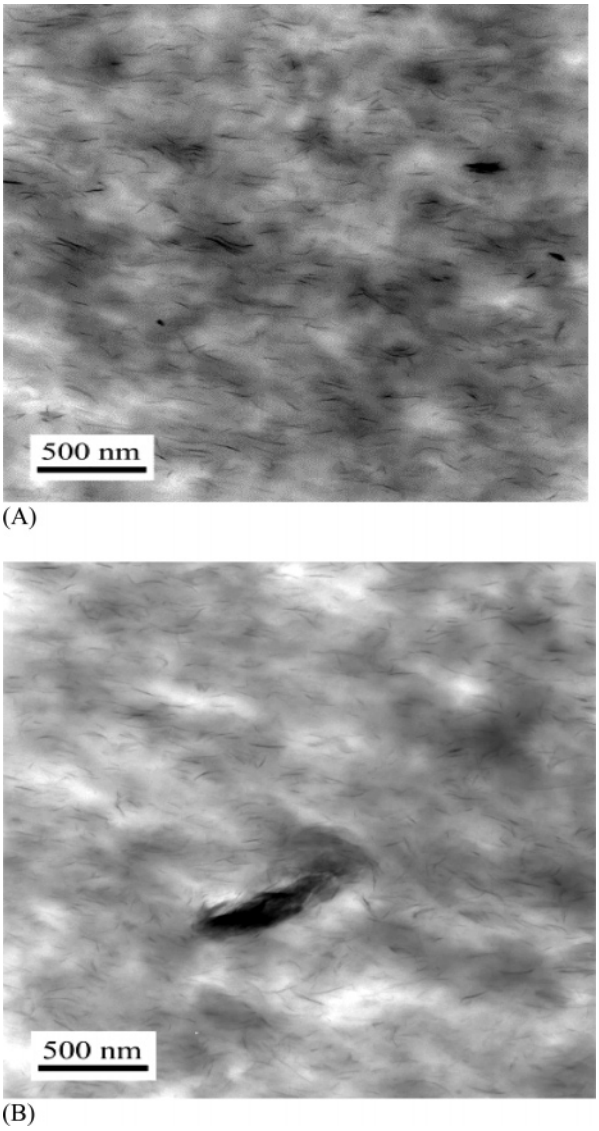

Figure 1. TEM pictures of 4% 30B clay/nylon-11 nanocomposite feature a partial exfoliated microstructure with the presence of larger tactoids.

2. Electric Modulus. The dc conductivity that was observed in the high-temperature data of Figures 3 and 4 is associated with the transport of free ions through the softened polymer matrix under the action of an electric field. By using the electric modulus formalism[60] for the treatment of raw dielectric data, the contribution of electrode screening and conductivity effects in the low-frequency tail can be minimized.[61] To better identify the high-temperature relaxation process, the electric moduli (M'') at various temperatures are computed by dividing the raw dielectric loss data, ϵ'', by $\epsilon''^2 + \epsilon'^2$ and are plotted against temperature, as shown in Figure 5A. The M'' peaks, detected within the experimental frequency window, denote an α relaxation process which is associated with the glass−rubber transition of the nylon-11 matrix.

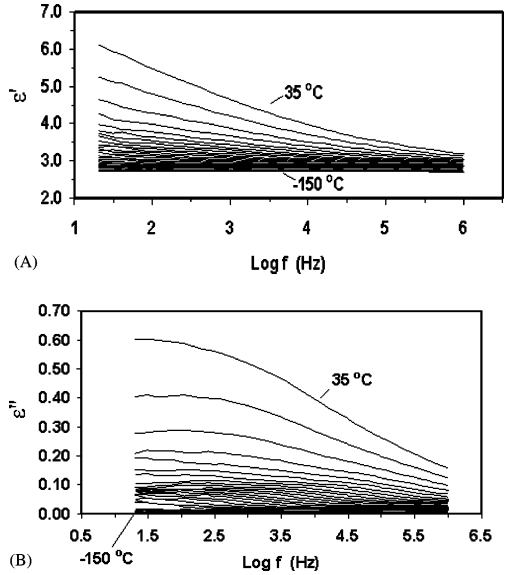

Figure 2. (A) ϵ' vs log f between −150 and 35 °C. (B) ϵ'' vs log f between −150 and 35 °C for neat nylon-11. The data were obtained at 5 °C intervals.

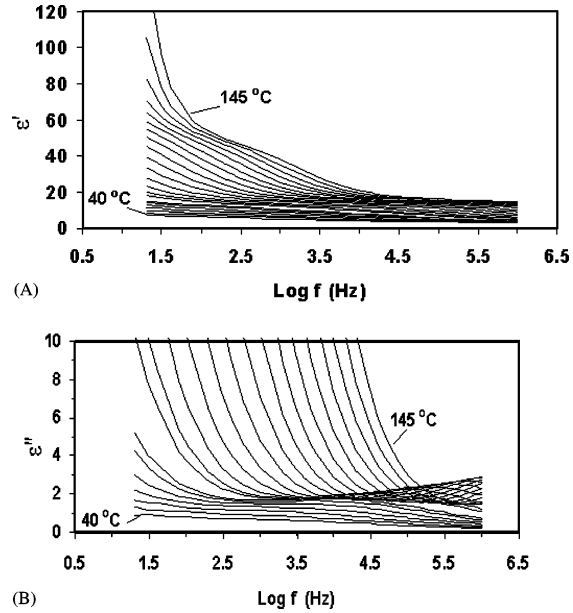

Figure 3. (A) ϵ' vs log f between 40 and 145 °C. (B) ϵ'' vs log f between 40 and 145 °C for neat nylon-11. The data were obtained at 5 °C intervals. Electrode polarization effects are expressed in the ϵ' data for temperatures above 140 °C. The α, α_w, and β relaxations are seen in these data. Large dc conductivity obscures the α relaxation in the ϵ'' plot.

The relaxation frequencies obtained from the maxima of M'' in Figure 5A are plotted against reciprocal temperature as seen in Figure 5B. Clay-filled nylon-11 yields a higher α relaxation frequency compared to the neat resin for the entire temperature range studied. Flat silicate platelets divide the bulk polymer chains into smaller domains, thus reducing the intermolecular cooperativity between polymer chains and accelerating the α dynamics. This reduced cooperative motion in the composite system manifests upon decreasing temperature toward the glass transition as indicated by the difference in relaxation times ($\tau_{neat} - \tau_{30B}$), also shown in Figure 5B. It is well documented that the size of cooperative domain increases with decreasing temperature.[62−64] Thus, a greater number of molecules

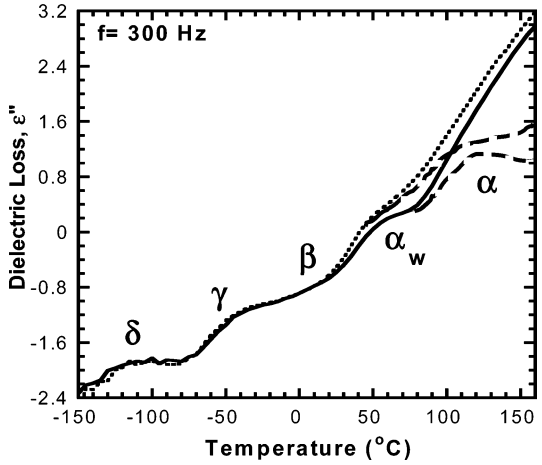

Figure 4. Dielectric loss (ϵ'') measured at frequency of 300 Hz is plotted against temperature for the neat nylon-11 (solid lines) and its 30B nanocomposite (short dashed curve). The long dashed curves denote the raw data for which the dc conductivity has been subtracted.

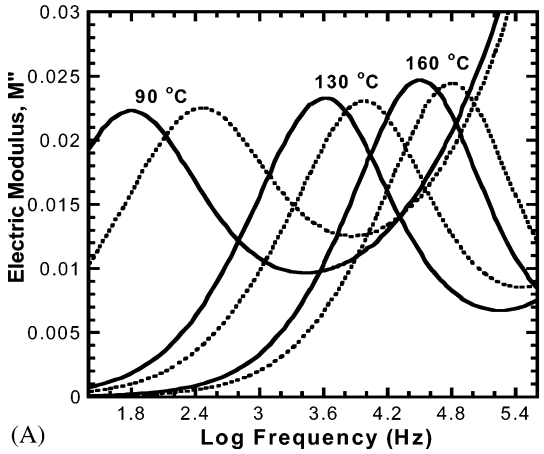

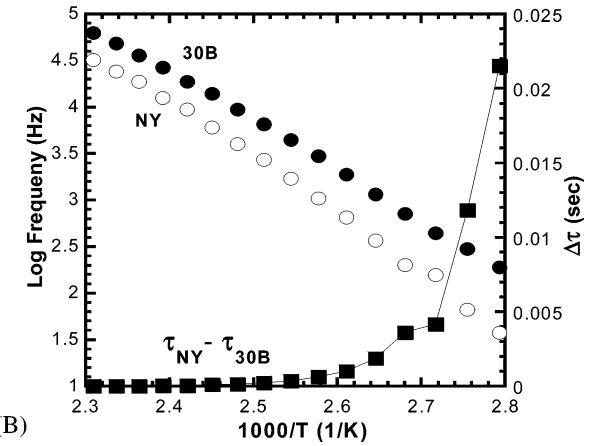

Figure 5. (A) Electric loss modulus (M'') is plotted against frequency in the semilogarithmic scale at three temperatures for the neat nylon-11 (solid lines) and for its 30B composite (dashed lines). (B) Peak frequencies of α relaxation determined from M'' are plotted against reciprocal temperature, and the difference in relaxation time scale between the neat nylon-11 and its composite is also included.

in the neat system are able to relax simultaneously in a cooperative motion at lower temperatures approaching the glassy state. It is proposed that the cooperative

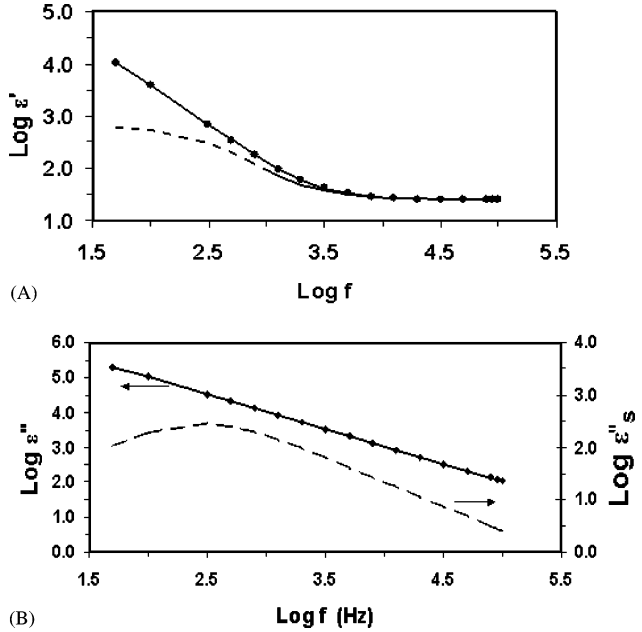

Figure 6. (A) Log ϵ' vs log f and (B) log ϵ'' vs log f are plotted for neat nylon-11 during extrusion at 195 °C. Points are measured data. Solid lines are curve fits to the data. The dashed curve of (A) is ϵ' of the material obtained upon correcting the data for electrode polarization, and the dashed curve of (B) is ϵ'' of the material that was obtained from the curve fitting where ϵ''_s is the dielectric loss after subtraction of the dc conductivity. One relaxation with characteristic frequency log $f = 2.50$ was obtained from the fit. The average curve fitting error for these data is 0.30%.

domain size in the nanocomposite compared to that in the neat resin did not enlarge much as temperature decreases because some of the polymer chains are segregated between silicate plates. In other words, the sizes of the cooperative domains in the exfoliated 30B/nylon are defined by the space between rigid silicate walls.

3. Melt State Properties. Curve fittings to the dielectric data of the melt state for both neat resin and its composite are shown in Figures 6 and 7. The relaxations retrieved from the fit are shown in Figure 8, and the fitting parameters are summarized in Table 1. The only relaxation detected in the molten nylon-11 is associated with the α relaxation. The incorporation of filler does not alter the α dynamics in the melt state as identical characteristic frequencies and similar relaxation time distributions are calculated for the composite and the neat sample. The only variation found in α relaxation is a higher dielectric intensity ($\Delta\epsilon_\alpha$) in the composite compared to the neat nylon, which is attributed to the extra molecular dipoles formed by the hydrogen bonds between the polar surfactants in 30B clay and the amide groups from the nylon matrix. In addition to the α relaxation, a Maxwell−Wagner−Sillars interfacial polarization[43−45] is observed in the composite, which occurred due to the charge accumulation at the resin/filler interface. MWS dispersion can be distinguished from the α relaxation by its larger intensity ($\Delta\epsilon_{MWS}$) and a much broader relaxation time distribution (δ_{MWS}). The magnitude of the MWS relaxation derived from the conducting ions is much greater than that for the α relaxation in the neat nylon-11 produced by orientation of the molecular dipoles.

4. The Log Frequency vs Reciprocal Temperature Relaxation Map. Examples of curve fitting to the

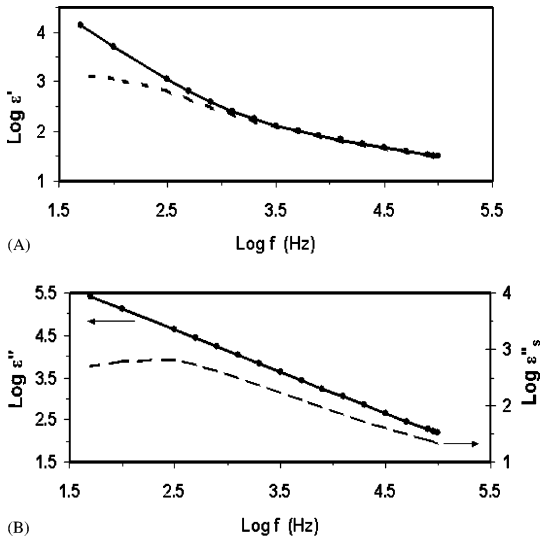

Figure 7. (A) Log ϵ' vs log f and (B) log ϵ'' vs log f are plotted for nylon-11/30B composite during extrusion at 195 °C. Points are measured data. Solid lines are curve fits to the data. The dashed curve of (A) is ϵ' of the material obtained upon correcting the data for electrode polarization, and the dashed curve of (B) is ϵ''_s, the dielectric loss of the material obtained from curve fitting and subtraction of the dc conductivity. Two relaxations with characteristic frequencies of log $f = 0.70$ and log $f = 2.50$ were obtained from the fit. The average curve fitting error for these data (ϵ' and ϵ'') is 0.31%.

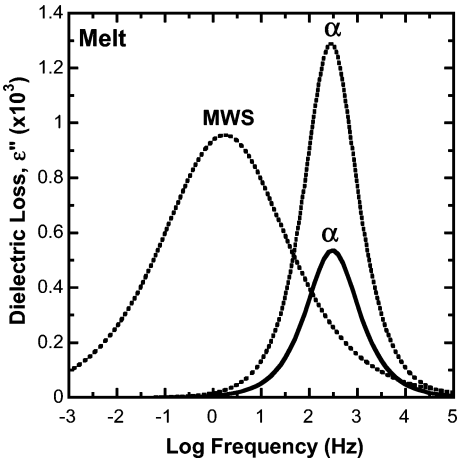

Figure 8. MWS and α relaxations retrieved from dielectric loss data (ϵ'') in the melt state at 195 °C are plotted against log frequency for the neat nylon-11 (solid line) and its 30B composite (dashed line).

off-line data at 130 and 70 °C for both neat and composite materials are shown in Figures 9−12. Of the four examples shown, the highest average error between the fit and the measurement is 0.31%. The quality of the curve fitting underscores the precision with which we were able to extract the relaxation parameters from these data. A prominent difference between the two temperatures is the large electrode polarization that is observed in the ϵ' data for the composite at 130 °C, whereas electrode polarization is absent from the data at 70 °C, a temperature close to T_g. The relaxation frequencies retrieved by the fitting procedure from both off-line and on-line measurements are plotted against reciprocal temperature for the neat nylon and its composite in Figure 13A,B. Six relaxation modes are assigned, five of which are seen in the raw data of Figure 4. The sixth relaxation is the MWS interfacial polarization, which is absent from the 300 Hz data of

Table 1. Summary of On-line Curve-Fitting Including Frequency, Dielectric Strength, Relaxation Time Distribution, and dc Conductivity[a]

nylon-11	neat	30B
structure		exfoliated
$\log f_\alpha$ (Hz) at 195 °C	2.49 ± 0.04	2.49 ± 0.07
$\log f_{MWS}$ (Hz) at 195 °C		0.65 ± 0.07
$\Delta\epsilon_\alpha$	1143 ± 40	2052 ± 900
$\Delta\epsilon_{MWS}$		3348 ± 900
δ_α	0.077 ± 0.01	0.074 ± 0.02
δ_{MWS}		0.51 ± 0.02
$\sigma_{dc} \times 10^3$ (S/m)	0.90 ± 0.02	1.11 ± 0.01
T_g (°C)[b]	56	29
T_g (°C)[c]	68	53
T_g (°C)[d]	90	66

[a] The dc conductivity and the α and α_w relaxation frequencies are fitted by using the VTF equation[72−74] fitting, and the T_g was then estimated from T_v, which is one of the fitting parameters. [b] T_g estimated from dc conductivity. [c] T_g estimated from α relaxation. [d] T_g estimated from α_w relaxation.

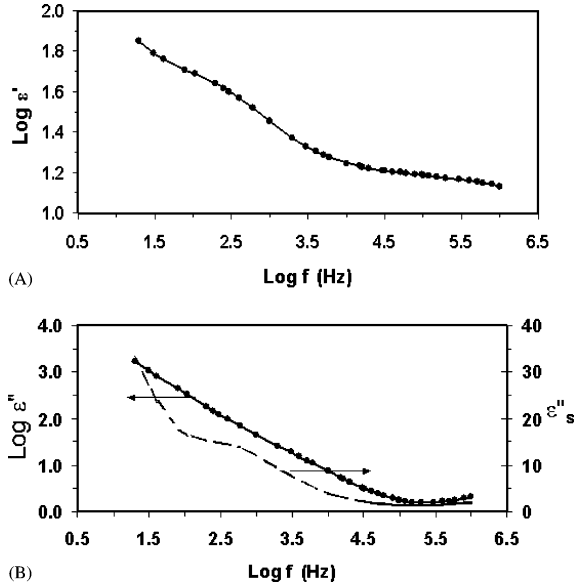

Figure 9. (A) Log ϵ' vs log f and (B) log ϵ'' vs log f are plotted for neat nylon-11 at 130 °C. Points are measured data. Solid line is the curve fit to the data. The dashed curve is ϵ_s'' of the material that was obtained from curve fitting where ϵ_s'' is the dielectric loss after subtraction of the dc conductivity. Three relaxations with characteristic frequencies at log $f = 1.00$, log $f = 2.69$, and log $f = 7.05$ were obtained from the fit. The average curve fitting error for these data (ϵ' and ϵ'') is 0.14%.

Figure 4 because it occurs at a much lower frequency. Relaxation frequencies increase with rising temperature for all the relaxation modes, except for MWS, as thermal energy in conjunction with a lower viscosity at the elevated temperature assist the molecular dipoles to follow the alternating electric field. Not much difference between the neat polymer and the composite is observed in the secondary or low-temperature relaxation process (β, γ, and δ); thus, we will focus our discussion on the primary α relaxation and the MWS interfacial polarization throughout this study.

Strikingly, slower α chain dynamics were detected in the melt state compared to the solid semicrystalline state of nylon-11 and its composite system. This is because the densely packed crystalline domains in the solid nylon matrix, between which amorphous chains are segregated, diminish the intermolecular cooperativity of the macromolecules. Thus, a much higher α relaxation frequency of the semicrystalline state over

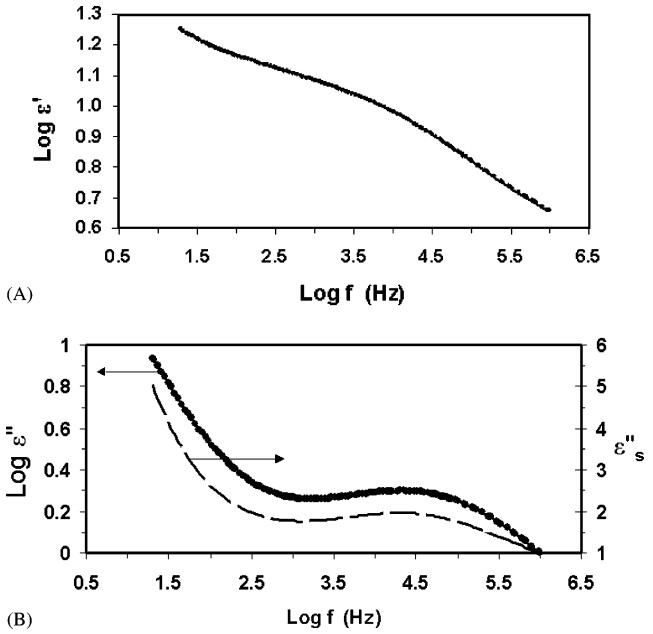

Figure 10. (A) Log ϵ' vs log f and (B) log ϵ'' vs log f are plotted for neat nylon-11 at 70 °C. Points are measured data. Solid line (obscured by data points) is the curve fit to the data. The dashed curve is ϵ_s'' of the material that was obtained from curve fitting where ϵ_s'' is the dielectric loss after subtraction of the dc conductivity. Three relaxations with characteristic frequencies at log $f = -0.45$, log $f = 2.82$, and log $f = 4.50$ were obtained from the fit. The average curve-fitting error for these data (ϵ' and ϵ'') is 0.18%.

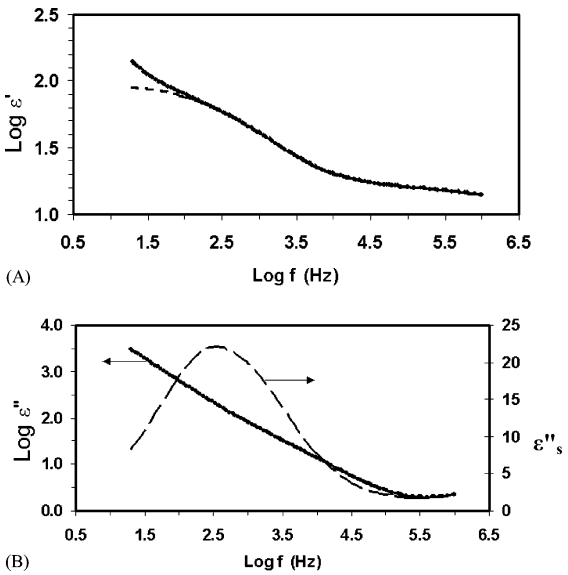

Figure 11. (A) Log ϵ' vs log f and (B) log ϵ'' vs log f are plotted for nylon-11/30B composite at 130 °C. Points are measured data. Solid line (obscured by data points) is the curve fit to the data. The dashed curve of (A) is ϵ' of the material after correction for electrode polarization. The dashed curve of (B) is ϵ_s'', the dielectric loss of the material that was obtained from curve fitting and subtraction of the dc conductivity. Three relaxations with characteristic frequencies at log $f = 2.34$, log $f = 3.215$, and log $f = 7.125$ were obtained from the fit. The average curve-fitting error for these data (ϵ' and ϵ'') is 0.11%.

the melt state is observed. This observation is in agreement with observations by Laredo, who observed that the glass transition in polycarbonate decreased with increasing crystallinity,[65] but is contrary to what has been observed in poly(ethylene terephthalate) (PET),[56,66] poly(aryl ether ketone ketone) (PAEK),[5] and

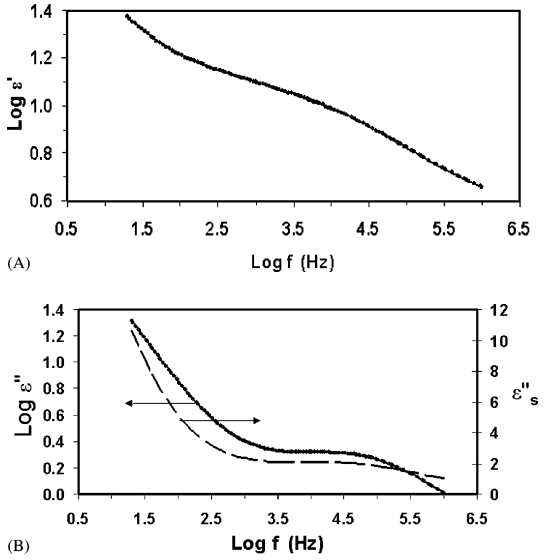

Figure 12. (A) Log ϵ' vs log f and (B) log ϵ'' vs log f are plotted for nylon-11/30B composite at 70 °C. Points are measured data. Solid line (obscured by data points) is the curve fit to the data. The dashed curve is ϵ''_s, the dielectric loss of the material that was obtained from curve fitting and subtraction of the dc conductivity. Three relaxations with characteristic frequencies at log $f = 0.59$, log $f = 3.51$, and log $f = 4.69$ were obtained from the fit. The average curve-fitting error for these data (ϵ' and ϵ'') is 0.18%.

poly(L-lactide).[67] The impact on α dynamics due to crystallization can involve several phenomena: diminished intermolecular cooperativity, hindered rotational motion at the amorphous/crystal interface, and confinement of amorphous molecules to regions smaller than the correlation length describing α dynamics.[68,69] Diminished intermolecular cooperativity and confinement of molecules will increase the characteristic frequencies of α dynamics, whereas hindered motion will have the opposite effect tending to decrease the characteristic frequencies of α dynamics. The changes in relaxation dynamics for nylon-11 upon crystallization indicate that diminished intermolecular cooperativity and/or the confinement of amorphous molecules are dominant. This interpretation is supported by Boyd and Yemni, who found that the intermolecular dipole−dipole correlation factor in nylon-6−10 was significantly higher for the amorphous melt than for the amorphous phase of the semicrystalline state.[70] For PET, PAEK, and poly L-lactide, hindered motion of the amorphous component by microcrystals slows the α dynamics and raises T_g, but for the nylons where hydrogen bonding plays a prominent role in molecular dynamics, diminished intermolecular cooperativity that accompanies a change in hydrogen bonding dominate effects due to crystallization.

5. Solid-State Properties—Impact of Filler on α and MWS Relaxations. Three relaxation modes, MWS, α, and α_w, were retrieved from the dielectric raw data in the solid semicrystalline state at 130 °C, as illustrated in Figure 13A,B. The curve-fitted dielectric loss (ϵ'') at 130 °C is depicted as a function of log frequency for both neat nylon and its composite in Figure 14A. No distinguishable differences can be found between the neat nylon and the composite for α_w relaxation; thus, only MWS and α are shown in the plot. Three interesting features are worth mentioning. First, the relaxation time distribution for the MWS interfacial polarization is broader than that for the α relaxations for both

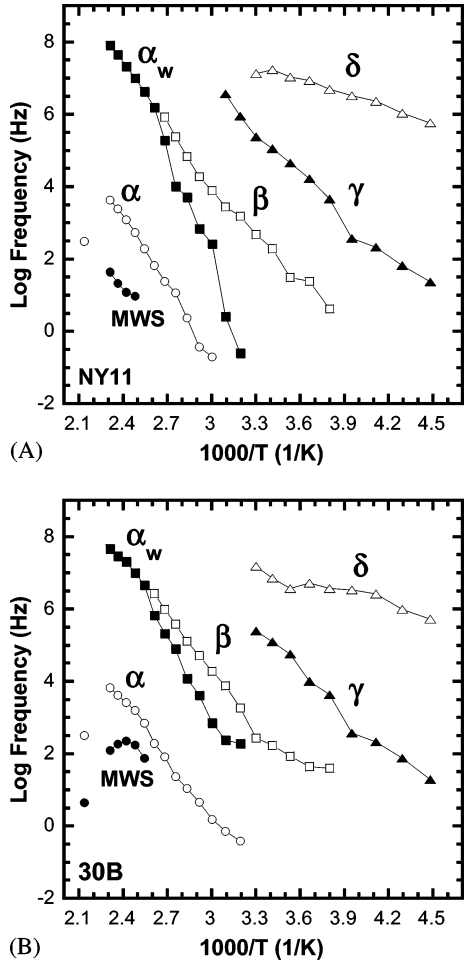

Figure 13. Arrhenius plot of (A) nylon-11 and (B) its 30B composite. Characteristic relaxation frequency is plotted against the reciprocal temperature in a semilogarithmic format.

systems. It is the heterogeneous geometry of the polymer/filler interfaces that is responsible for a range of different relaxation times. Second, a much higher dielectric intensity for MWS than that for the α relaxations is due to the distinct nature of these two relaxation modes. Much higher dielectric magnitude for MWS is produced upon polarization of ions piled up at the polymer/filler interfaces compared to the α dielectric intensity that arises from the alignments of molecular dipoles. Third, 30B nanocomposite exhibits much faster α relaxation dynamics with a narrower relaxation time distribution than the neat nylon-11. Again, it is the presence of delaminated silicates that segregate the bulk amorphous chains into smaller domains and hence diminish the intermolecular cooperativity.

Total relaxation strength, summed from three relaxation modes (α, α_w, and β), is plotted against reciprocal temperature in Figure 14B. In the temperature range between 130 and 160 °C, which is much greater than T_g and is below the melting temperature of nylon-11 (185 °C), the neat polymer behaves as a partially softened amorphous medium. Molecular dipoles can undergo free rotation; thus, thermal energy serves to randomize the dipole alignments. The positive slope derived from the relationship between the total dielectric strength and the reciprocal temperature in the neat nylon is indicative of this randomization of dipole moments due to thermal energy. In other words, the total dielectric intensity is proportional to $1/kT$. However, the clay-filled nanocomposite system is highly

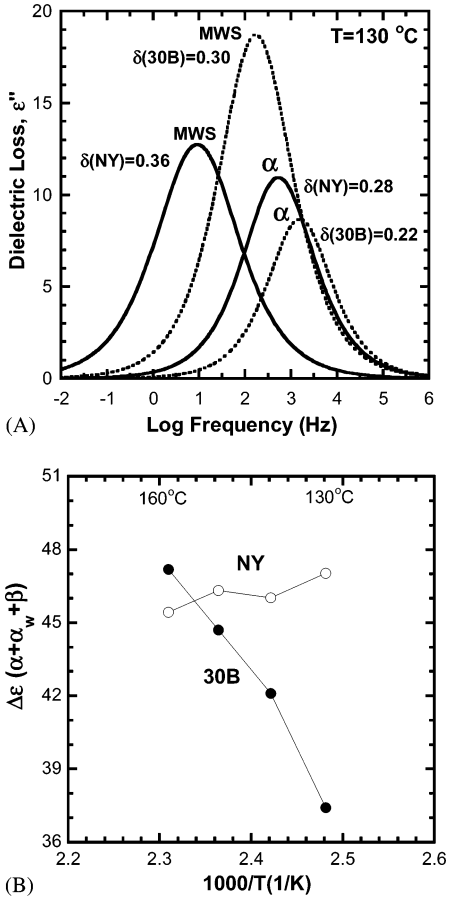

Figure 14. (A) MWS and α relaxation retrieved from dielectric loss data in the semicrystalline state at 130 °C are plotted against log frequency for the neat nylon-11 (solid line) and its 30B composite (dashed line). (B) Total dielectric relaxation strength, $\Delta\epsilon(\alpha + \alpha_w + \beta)$, summed from three relaxation modes (α, α_w, and β) is plotted against the reciprocal temperature for nylon-11 (open circles) and its 30B composite (filled circles).

heterogeneous compared to the neat nylon due to the presence of the rigid silicates. The temperature has an opposite effect on the total dielectric strength of the nanocomposite system compared to the neat nylon-11 as the negative slope is seen in the plot. Thermal energy facilitates the orientation of the molecular dipoles in the composite medium where hindered dipole rotation occurs.[5−9] The higher the temperature, the easier it is to rotate and align the molecular dipoles that are hindered by the presence of rigid silicate platelets.

6. Solid-State Properties—Impact of Filler on α and α_w Relaxations. Three relaxation modes are retrieved from the dielectric raw data at 70 °C, which include α, α_w, and β relaxations. Only α and α_w are displayed in Figure 15, as the local β relaxation in the exfoliated nanocomposite yielded no difference from the neat resin at 70 °C. Data obtained at 70 °C are in contrast to the observation at 130 °C where α_w relaxation parameters were identical for both neat and the composite. The impact of exfoliated filler on α and α_w dynamics at 70 °C is evident in both characteristic frequencies and relaxation time distribution. 30B nanocomposite exhibited a greater relaxation frequency with a narrower relaxation time distribution than the neat nylon-11 for both glass transition-related relaxations (α and α_w). As we stated above, the diminished intermolecular cooperativity in the nanocomposite allows the polymer chains to relax with a shorter time scale.

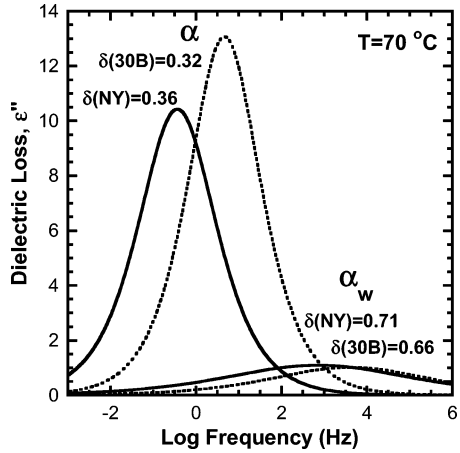

Figure 15. α_W and α relaxations retrieved from dielectric loss data in the semicrystalline state at 70 °C are plotted against log frequency for the neat nylon-11 (solid lines) and its 30B composite (dashed lines).

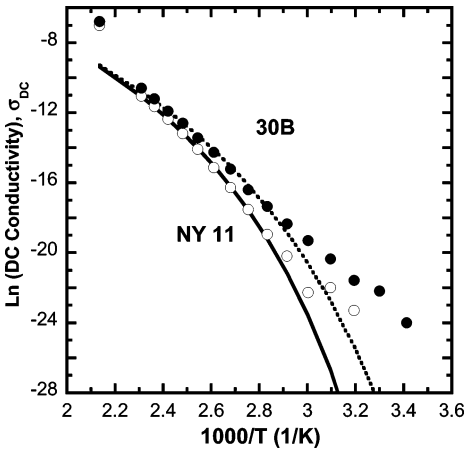

Figure 16. Dc conductivity is plotted against reciprocal temperature for nylon-11 (open circle) and its clay-filled composite (closed circle). The solid and the dashed lines are the Vogel−Tamman−Fulcher (VTF) fits to the nylon-11 and its composite data, respectively.

It is worth pointing out that the relaxation time distribution for the α_w is much broader than that for the α relaxations for both systems. This is a direct result of heterogeneity in α_w activated by the plasticized amorphous chains in the solid state.[39] Attention should also be drawn to the effect of temperature on the relaxation time distribution for both systems, which are broader at 70 °C ($\delta_\alpha = 0.36$ for nylon-11) than at 130 °C ($\delta_\alpha = 0.28$ for nylon-11). Upon approaching the glass transition temperature of the polymer matrix, a broadened distribution of relaxation times is expected. The coexistence of the nearly glassy and soften amorphous domains near T_g is responsible for the observed broadened relaxation time distribution at 70 °C.[71]

7. DC Conductivity. The dc conductivities for the neat nylon-11 and its composite are plotted against reciprocal temperature in Figure 16. The composite sample exhibits greater dc conductivity than the neat polymer, which is due to the presence of additional ions from the clay. The solid line in Figure 16 is the result of fitting the data with the VFT equation[72−74]

$$f = A \exp\left(\frac{B}{T - T_v}\right) \tag{7}$$

where A, B, and T_v are fitting parameters. A greater T_v

retrieved from VFT fitting for the neat polymer implied a higher glass transition temperature ($T_g \approx 1.33T_v$)[75] in the neat nylon-11 than in the composite. The T_g reduction in clay-filled nylon-11 nanocomposites has been reported in the literature where a 5 deg decrease in T_g was observed in nylon-11 containing 4% clay filler.[31]

Conclusions

The on-line dielectric sensor enables us to gain insights into how the relaxation dynamics of molten nylon-11 are altered upon the addition of exfoliated silicate filler. The present work reveals striking differences between the melt and the semicrystalline state properties. Five prominent features, which differentiate the clay-filled system from the neat nylon, are disclosed in our study. First, the higher characteristic frequency and a narrower relaxation time distribution for the α relaxation in the composite over the neat resin are due to diminished intermolecular cooperativity of the amorphous chains segregated by silicate particles. Second, higher relaxation strength for the α relaxation observed in the composite is attributed to the extra molecular dipoles formed through the hydrogen bonds between the polar surfactants and the amide groups. Third, higher dc conductivity in the nanocomposite compared to the neat resin is a direct result of incorporated ionic surfactants in the filler. Fourth, only one relaxation (α) can be identified in the molten nylon-11, yet two relaxation modes (α and MWS) are retrieved from the composite melt. MWS is an interfacial polarization, associated with the polymer/filler interfaces, and possesses a significantly greater dielectric magnitude with a much broader relaxation time distribution compared to the α relaxation which derives from the reorientation of molecular dipoles. Finally, randomization of molecular dipoles upon increasing temperature is observed in the neat nylon yet absent from the composite, which suggests a hindered dipole rotation in the semicrystalline state above T_g due to the presence of rigid fillers.

References and Notes

(1) Schwartz, G. A.; Bergman, R.; Swenson, J. *J. Chem. Phys.* **2004**, *120*, 5736−5744.
(2) Swenson, J.; Schwartz, G. A.; Bergman, R.; Howells, W. S. *Eur. Phys. J. E* **2003**, *12*, 179−183.
(3) Schwartz, G. A.; Bergman, R.; Mattsson, J.; Swenson, J. *Eur. Phys. J. E* **2003**, *12*, S113−S116.
(4) Anastasiadis, S. H.; Karatasos, K.; Vlachos, G.; Manias, E.; Giannelis, E. P. *Phys. Rev. Lett.* **2000**, *84*, 915−918.
(5) Ezquerra, T. A.; Majszczyk, J.; Baltacalleja, F. J.; Lopez-cabarcos, E.; Gardner, K. H.; Hsiao, B. S. *Phys. Rev. B* **1994**, *50*, 6023−6031.
(6) Hoffman, J. D.; Williams, G.; Passaglia, E. *J. Polym. Sci., Part C* **1966**, *14*, 173−235.
(7) Korbakov, N.; Harel, H.; Feldman, Y.; Marom, G. *Macromol. Chem. Phys.* **2002**, *203*, 2267−2272.
(8) Nuriel, H.; Kozlovich, N.; Feldman, Y.; Marom, G. *Composites, Part A* **2000**, *31*, 69−78.
(9) Scott, A. H.; Scheiber, D. J.; Curtis, A. J.; Hoffman, J. D. *J. Res. Natl. Bur. Stand.* **1962**, *66A*, 269−305.
(10) Simha, R.; Boyer, R. F. *J. Chem. Phys.* **1962**, *37*, 1003.
(11) Bohmer, R.; Ngai, K. L.; Angell, C. A.; Plazek, D. J. *J. Chem. Phys.* **1993**, *99*, 4201−4209.
(12) Ngai, K. L.; White, C. T. *Phys. Rev. B* **1979**, *20*, 2475−2486.
(13) Ngai, K. L.; Jonscher, A. K.; White, C. T. *Nature (London)* **1979**, *277*, 185−189.
(14) Ngai, K. L.; Roland, C. M. *Macromolecules* **1993**, *26*, 6824−6830.
(15) Ngai, K. L.; Roland, C. M. *Macromolecules* **1993**, *26*, 2688−2690.
(16) Ngai, K. L.; Plazek, D. J. *Rubber Chem. Technol.* **1995**, *68*, 376−434.
(17) Plazek, D. J.; Ngai, K. L. *Macromolecules* **1991**, *24*, 1222−1224.
(18) Roland, C. M.; Ngai, K. L. *Macromolecules* **1992**, *25*, 363−367.
(19) Angell, C. A.; Moynihan, C. T.; Hemmati, M. *J. Non-Cryst. Solids* **2000**, *274*, 319−331.
(20) Huth, H.; Beiner, M.; Donth, E. *Phys. Rev. B* **2000**, *61*, 15092−15101.
(21) Donth, E.; Kahle, S.; Korus, J.; Beiner, M. *J. Phys. I* **1997**, *7*, 581−598.
(22) Saito, H.; Miyashita, H.; Inoue, T. *Macromolecules* **1992**, *25*, 1824−1827.
(23) Angell, C. A. *J. Non-Cryst. Solids* **1991**, *131*, 13−31.
(24) Matsuoka, S.; Quan, X. *J. Non-Cryst. Solids* **1991**, *131*, 293−301.
(25) Neagu, R. M.; Neagu, E.; Kyritsis, A.; Pissis, P. *J. Phys. D: Appl. Phys.* **2000**, *33*, 1921−1931.
(26) Rhee, S.; White, J. L. *J. Polym. Sci., Part B: Polym. Phys.* **2002**, *40*, 2624−2640.
(27) Frubing, P.; Kremmer, A.; Neumann, W.; Gerhard-Multhaupt, R. *IEEE Trans. Dielectr. Electr. Insul.* **2004**, *11*, 271−279.
(28) Zhang, G. S.; Li, Y. J.; Yan, D. Y. *J. Polym. Sci., Part B: Polym. Phys.* **2004**, *42*, 253−259.
(29) Neagu, E. R.; Marat-Mendes, J. N.; Dias, C. J. *Ferroelectrics* **2003**, *294*, 3−11.
(30) Neagu, R. M.; Marat-Mendes, J. N.; Neagu, E. R.; Pissis, P. *Ferroelectrics* **2003**, *294*, 113−122.
(31) Liu, T. X.; Lim, K. P.; Tjiu, W. C.; Pramoda, K. P.; Chen, Z. K. *Polymer* **2003**, *44*, 3529−3535.
(32) Hong, S. C.; Zhang, C.; Shen, Y. R. *Appl. Phys. Lett.* **2003**, *82*, 3068−3070.
(33) Bizet, A.; Nakamura, N.; Teramoto, Y.; Hatakeyama, T. *Thermochim. Acta* **1994**, *237*, 147−157.
(34) Boutros, S.; Rizk, H. A.; Hanna, A.; Gerges, M. K. *J. Chim. Phys. Phys.-Chim. Biol.* **1979**, *76*, 501−506.
(35) Laredo, E.; Grimau, M.; Sanchez, F.; Bello, A. *Macromolecules* **2003**, *36*, 9840−9850.
(36) McCall, D. W.; Anderson, E. W. *J. Chem. Phys.* **1960**, *32*, 237−241.
(37) Sauer, J. A.; Lim, T. *J. Macromol. Sci., Phys.* **1977**, *B13*, 419−439.
(38) Xin, N.; Ishida, H. S. *J. Polym. Sci., Part B: Polym. Phys.* **1991**, *29*, 1479−1492.
(39) Laredo, E.; Hernandez, M. C. *J. Polym. Sci., Part B: Polym. Phys.* **1997**, *35*, 2879−2888.
(40) Frank, B.; Frubing, P.; Pissis, P. *J. Polym. Sci., Part B: Polym. Phys.* **1996**, *34*, 1853−1860.
(41) Hanna, A. A. *Thermochim. Acta* **1984**, *76*, 97−103.
(42) Kapur, S.; Rogers, C. E.; Baer, E. *J. Polym. Sci., Polym. Phys.* **1972**, *10*, 2297−2300.
(43) Maxwell, J. C. *Electricity and Magnetism*; Clarendon: Oxford, 1892.
(44) Sillars, R. W. *J. Inst. Electr. Eng.* **1937**, *80*, 378.
(45) Wagner, K. W. *Arch. Elektrotech.* **1914**, *2*, 371.
(46) Jolly, L.; Tidu, A.; Heizmann, J. J.; Bolle, B. *Polymer* **2002**, *43*, 6839−6851.
(47) Bur, A. J.; Roth, S. C.; Lee, Y. H.; McBrearty, M. *Rev. Sci. Instrum.* **2004**, *75*, 1103−1109.
(48) Bur, A. J.; Roth, S. C.; McBrearty, M. *Rev. Sci. Instrum.* **2002**, *73*, 2097−2102.
(49) Perusich, S.; McBrearty, M. *Polym. Eng. Sci.* **2000**, *40*, 214−226.
(50) Zaretsky, M. C.; Li, P.; Melcher, J. R. *IEEE Trans. Electr. Insul.* **1989**, *24*, 1159−1166.
(51) Pizzitutti, F.; Bruni, F. *Rev. Sci. Instrum.* **2001**, *72*, 2502−2504.
(52) Cole, R. H. *J. Chem. Phys.* **1955**, *23*, 493.
(53) Havriliak, S.; Negami, S. *J. Polym. Sci., Part C: Polym. Symp.* **1966**, *14*, 99.
(54) Boyd, R. H.; Porter, C. H. *J. Polym. Sci., Part A-2* **1972**, *10*, 647−656.
(55) Boyd, R. H. *Polymer* **1985**, *26*, 323−347.
(56) Coburn, J. C.; Boyd, R. H. *Macromolecules* **1986**, *19*, 2238−2245.
(57) Ryabov, Y. E.; Nuriel, H.; Marom, G.; Feldman, Y. *J. Polym. Sci., Part B: Polym. Phys.* **2003**, *41*, 217−223.
(58) Huo, P. T.; Cebe, P. *J. Polym. Sci., Part B: Polym. Phys.* **1992**, *30*, 239−250.
(59) Gauthier, C.; Chailan, J. F.; Chauchard, J. *Makromol. Chem., Macromol. Chem. Phys.* **1993**, *194*, 1421−1434.

(60) Macedo, P. B.; Moynihan, C. T.; Simmons, J. H.; Bose, R. *Phys. Chem. Glasses* **1972**, *13*, 171−179.
(61) Kanapitsas, A.; Pissis, P.; Estrella, A. G. *Eur. Polym. J.* **1999**, *35*, 923−937.
(62) Adam, G.; Gibbs, J. H. *J. Chem. Phys.* **1965**, *28*, 373.
(63) Arndt, M.; Stannarius, R.; Groothues, H.; Hempel, E.; Kremer, F. *Phys. Rev. Lett.* **1997**, *79*, 2077−2080.
(64) Matsuoka, S. *J. Res. Natl. Inst. Stand. Technol.* **1997**, *102*, 213−228.
(65) Laredo, E.; Grimau, M.; Muller, A.; Bello, A.; Suarez, N. *J. Polym. Sci. Part B: Polym. Phys.* **1996**, *34*, 2863−2879.
(66) Williams, G. *Adv. Polym. Sci.* **1979**, *33*, 59.
(67) Kanchanasopa, M.; Runt, J. *Macromolecules* **2004**, *37*, 863−871.
(68) Ngai, K. L. *Eur. Phys. J. E* **2002**, *8*, 225−235.
(69) Ngai, K. L. *Eur. Phys. J. E* **2003**, *12*, 93−100.
(70) Yemni, T.; Boyd, R. H. *J. Polym. Sci., Part B: Polym. Phys.* **1976**, *14*, 499−508.
(71) Nayak, S. K.; Jena, P.; Ball, K. D.; Berry, R. S. *J. Chem. Phys.* **1998**, *108*, 234−239.
(72) Fulcher, G. S. *J. Am. Ceram. Soc.* **1925**, *8*, 339.
(73) Tammann, G.; Hesse, W. Z. *Anorg. Allg. Chem.* **1926**, *156*, 245.
(74) Vogel, H. *Phys. Z.* **1921**, *22*, 645.
(75) Zhukov, S.; Geppert, S.; Stuhn, B.; Staneva, R.; Ivanova, R.; Gronski, W. *Macromolecules* **2002**, *35*, 8521−8530.

MA048052M